IN THIS ISSUE:
The extended chain compounds $Ln_{12}(C_2)_3I_{17}$
(Ln = Pr, Nd, Gd, Dy): Synthesis, structure and
physical properties

M. Ryazanov, H. Mattausch A. Simon

Available online at
ScienceDirect
www.sciencedirect.com

JSSC

Structural and optical properties of ZnMgO nanostructures formed by Mg in-diffused ZnO nanowires

Ching-Ju Pan, Hsu-Cheng Hsu[1], Hsin-Ming Cheng[2], Chun-Yi Wu[3], Wen-Feng Hsieh*

Department of Photonics and Institute of Electro-Optical Engineering, National Chiao Tung University, 1001 Tahsueh Rd., Hsinchu 30050, Taiwan, Republic of China

Abstract

ZnMgO nanostructures with wurtzite phase were prepared by thermal diffusion of Mg into the ZnO nanowires. As ZnO light-emitting devices have been operated by using ZnMgO layers as energy barrier layers to confine the carriers, it is essential to realize the characterization of ZnMgO particularly. In this work, the Mg content in $Zn_{1-x}Mg_xO$ alloy determined by X-ray diffraction (XRD) and photoluminescence (PL) shows a good coincidence. The variation of lattice constant and the blueshift of near-band-edge emission indicate that Zn^{2+} ions are successfully substituted by Mg^{2+} ions in the ZnO lattice. In Raman-scattering studies, the change of E_2(high) phonon line shape in ZnO:Mg nanostructures reveals the microscopic substitutional disorder. In addition to the host phonons of ZnO, two additional bands around 383 and $510\,cm^{-1}$ are presumably attributed to the Mg-related vibrational modes.
© 2007 Elsevier Inc. All rights reserved.

Keywords: Photoluminescence; Raman spectroscopy; ZnO

1. Introduction

Among wide-band gap semiconductor materials, a pronounced advantage for ZnO (3.37 eV) is its large exciton binding energy ($\sim$60 meV) so that it has been recognized as a promising candidate for the development of short-wavelength photonic devices such as ultraviolet detectors, light-emitting diodes, and laser diodes. Additionally, band gap engineering has played an important role in modern optoelectronics since the emergence of superlattices (SLs) and quantum wells for carrier confinement. For example, Lim et al. [1] demonstrated the operation of the ZnO light-emitting devices emitted 380 nm UV light at room temperature (RT) with a turn-on voltage of 3.2 V. The intensity of near band edge (NBE) emission was increased further and greatly suppressed the deep level emission by using $Mg_{0.1}Zn_{0.9}O$ layers as energy barrier layers to confine the carriers to the high-quality n-type ZnO. $ZnO/Mg_{0.2}Zn_{0.8}O$ coaxial nanorod single quantum well structures were reported by Bae et al. [2], who proposed that the quantum confinement effect would depend on the $Mg_{0.2}Zn_{0.8}O$ barrier layer thickness as well as the ZnO well layer thickness. Fabrication and characterization of (Mg,Zn)O alloys are important from the viewpoint of band gap modulation as well as of p–n junction.

Raman spectroscopy is a versatile technique for fast and nondestructive study of dopant incorporation, particularly when impurity-induced modes can be traced back to individual constituents. Recently, Kaschner et al. [3] observed anomalous modes (AMs) at about 275, 510, 582, and $643\,cm^{-1}$ in ZnO:N films and explained the occurrence as local vibrational modes (LVMs) due to vibrating nitrogen-related complexes, Bundesmann et al. [4] suggested the same additional modes resulting from the host lattice defects by intentionally doping Fe, Sb, and Al, in the ZnO thin films without N. However, Manjon et al. [5] considered that most of the observed AMs correspond

---

*Corresponding author. Fax: +886 3 5716631.

E-mail address: wfhsieh@mail.nctu.edu.tw (W.-F. Hsieh).

[1] Present address: National Taiwan University, Center for Condensed Matter Sciences 1 Roosevelt Road, Section 4, Taipei, Taiwan 106, ROC.

[2] Also at: Material and Chemical Research Laboratories, Industrial Technology Research Institute, Hsinchu 310, Taiwan, ROC.

[3] Present address: Epistar Corporation, 5 Li-hsin 5th Rd., Science-based Industrial Park, Hsinchu 300, Taiwan, ROC.

to wurtzite-ZnO silent modes allowed by the breakdown of the translational symmetry induced by defects and impurities based on their *ab initio* calculations [6]. Although several works of undoped- and doped-ZnO thin films observed the AMs in the Raman spectra, little was reported about the influence of magnesium incorporation on the lattice dynamics of ZnO. In this letter, we reported the synthesis of the ZnMgO nanostructures, which can be achieved simply by thermal diffusion of Mg into the ZnO nanowires prepared by a simple vapor transport method [7]. The Mg composition in $Zn_{1-x}Mg_xO$ alloy can be estimated roughly by X-ray diffraction (XRD) and photoluminescence (PL). Especially, magnesium-related AMs are observed by Raman spectra for the first time in ZnMgO system.

2. Experimental procedures

ZnO nanowires were synthesized in a simple vapor transport process mediated by "self-catalyst" vapor–liquid–solid (VLS) growth [8] in a horizontal quartz tube furnace. An alumina boat contained the *c*-plane sapphire (0001) substrate and zinc powder was positioned in the center of the quartz tube furnace. Pure Zn metal powder (99.999%) was used as the zinc vapor source. The tube first was evacuated to a pressure below 10 Torr using a mechanical pump; then, the furnace was heated to 550 °C at a rate of 50 °C/min and high-purity argon gas was injected into the quartz tube at a flow rate of 500 sccm during 1 h of growth. After the growth process was complete, the tube furnace was cooled slowly to RT in Ar-gas ambience.

Although the quartz tube furnace was evacuated to a pressure below 10 Torr, there still contains enough residual O_2 to react with the condensate Zn vapor to form ZnO_x ($x < 1$) in the initial period of nucleation [9]. Because the melting points of Zn and ZnO_x are approximately 419 °C, simultaneously, the liquid phase Zn or ZnO_x would serve as the eutectic solvent for the oxide species. The anisotropic growth of the crystal causes formation of a ZnO (further oxidation by the residual O_2) nanostructure with a high aspect ratio and the ZnO nanowires are preferentially oriented along the *c*-axis direction due to the growth rate being fastest in this direction.

The ZnO nanowires were then spin-coated by the solution prepared by the sol–gel approach using acetate of magnesium in a homogeneous aqueous reaction medium. Finally, the samples were sintered at 1000 °C for 2 h while diffusion occurred to form the alloy. The morphology of Mg in-diffused ZnO nanowires (ZMO nanostructures) was characterized by scanning electron microscopy (SEM). The crystal structure was performed using Bede D1 thin film X-ray diffractometer with grazing incident mode. The PL measurement was made using a 20 mW He–Cd laser at wavelength of 325 nm and the emission light was dispersed by a TRIAX-320 spectrometer and detected by a UV-sensitive photomultiplier tube.

Micro-Raman spectroscopy was carried out using frequency-doubled Yb:YAG laser ($\lambda = 515$ nm) as the pump source, and a Jobin-Yvon T64000 micro-spectrometer with a 1800 grooves/mm grating in the backscattering configuration was employed.

3. Results and discussion

The SEM images of the ZMO nanostructures and ZnO nanowires having the same magnification are presented in Fig. 1 and its inset. The morphology of the ZnO nanowires (see the inset) displayed nearly well-aligned nanowires uniformly distributed over the entire substrate; most of them were grown with length and diameters ranging about 1–2 μm and 100–200 nm, respectively. The ZMO nanostructures consisted of fused filaments, which bundled several nanowires approximately 600–900 nm in diameter. Based on the SEM photographs, the cause of topological change of the obtained structures is illustrated as follows. According to the report of Hsu et al. [10], the formation of heterostructured ZnMgO alloy nanowires should result from post-heat treatment of the as-grown ZnO/MgO core-shell structure. In this experiment, in order to obtain the preformed ZnO/MgO core-shell structure, one would expect the solution could spread evenly on the outer layer of the nanowires by capillarity during the spin-coating process, whereas the excess solution had capped on top of the nanowires. After post-annealing treatment, Mg-based precipitates (see the bright region of the SEM image) on the head of fused nanowires correlated presumably with the above observation.

Shown in Fig. 2 are the XRD patterns of the ZMO nanostructures in comparison with the ZnO nanowires. For the ZMO nanostructures, all relatively sharp diffraction peaks can be indexed perfectly to a high crystallinity of hexagonal phase of ZMO with two small signals (denoted by open circles) attributed to MgO cubic phase. The appearance of a secondary phase was due to the
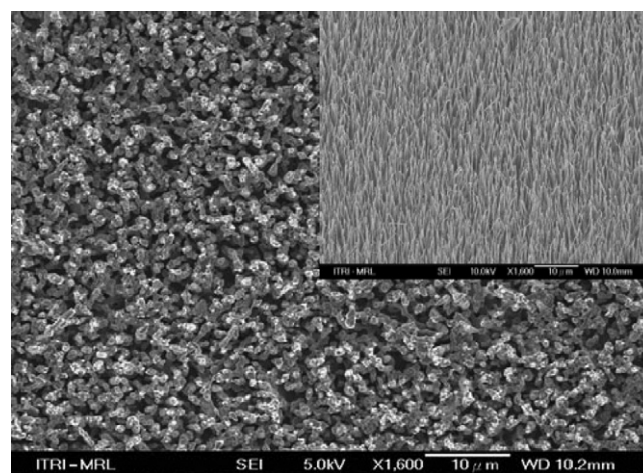

Fig. 1. The SEM images of the Mg in-diffused ZnO nanowires. The inset shows the original aligned ZnO nanowires.
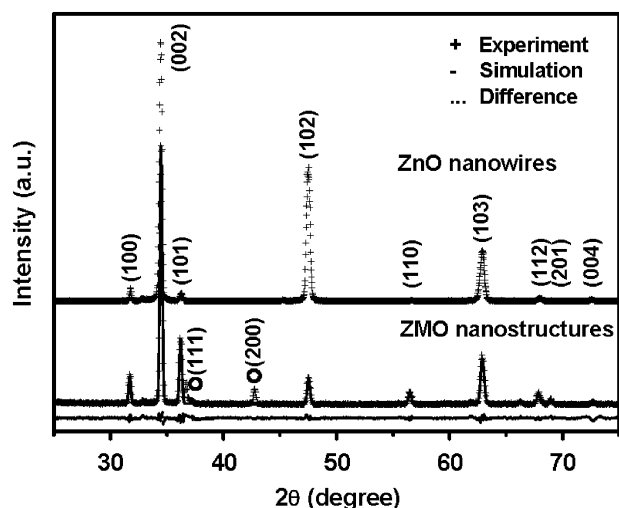
Fig. 2. The Rietveld refinement plot of ZMO nanostructures and ZnO nanowires. The open circles indicate the MgO cubic diffraction peaks.

Fig. 3. The normalized room-temperature PL spectra of ZMO nano-structures (solid curve) and ZnO nanowires (short dash curve).

precipitates of MgO particles on the top of fused filaments, as described in the SEM image. Additionally, the observed diffraction data were analyzed, using Rietveld analysis software (GSAS), by taking into account the preferred orientation of (002) planes in both samples. The refinement results of ZMO nanostructures, which well fit to the data with $R_{wp} = 4.70\%$, also are shown in Fig. 2. The lattice constant a are refined to be 3.25394 and 3.25804 Å; c to be 5.21050 and 5.20251 Å, for ZnO nanowires and ZMO nanostructures, respectively. The similar dependence of the lattice constant on Mg concentration usually is common in $Zn_{1-x}Mg_xO$ systems [11–13]. Assume the lattice constant varies linearly following Vegard's law, we determined the Mg content to be $11.99 \pm 2.66\%$ and $8.24 \pm 0.07\%$ according to the relations $a = 3.25394 + 0.0342x$ and $c = 5.21050 - 0.097x$ that were deduced from Fig. 2 in Ref. [11]. Therefore, the variation of lattice constant suggests that Mg^{2+} is incorporated into the ZnO host lattice and occupies the lattice sites of Zn^{2+}.

Fig. 3 shows the normalized room-temperature (RT) PL spectra of the ZMO nanostructures (solid curve) and the ZnO nanowires (short dashed curve). Two PL bands can be observed in the two spectra, one being in the ultraviolet (UV) and the other in the green. The UV emission is assigned to the NBE emission, which originates from the free exciton emission and its replicas [7,14,15]. The broad green emission is commonly attributed to intrinsic deep-level defects in ZnO such as oxygen vacancy, interstitial zinc, antisite oxygen, and ionic dopants [16–19]. Compared with the ZnO nanowires, two obvious differences can be found: the shift of NBE peak position of ZMO nanos-tructures to the higher energy from 3.26 to ~3.43 eV and the increase of intensity of deep-level emission owing to the formation of ternary ZnMgO alloy via Mg diffusion. This blueshift cannot be caused by quantum confinement effects because the sizes of ZMO nanostructures are far larger
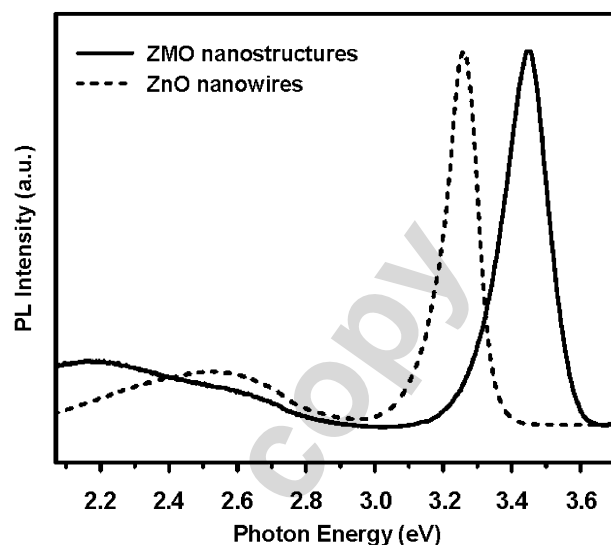
than the exciton Bohr radius (2.34 nm) of bulk ZnO. As a result, Mg doping should be responsible for such a blueshift. Additionally, the broadening of the NBE peak with the full-width at half-maximum (FWHM), with changing from 105 to 155 meV, is a result of the increase in fluctuation of composition and the lattice disorder in the alloy. The increasing deep-level emission probably comes from surface defects or lattice disorder caused by heat treatment. Therefore, due to the Mg incorporation, the ZMO nanostructures exhibit the blueshift of NBE peak position and the increased intensity of deep-level emission.

In order to demonstrate the homogeneity of our samples, we measured PL spectra at a dozen points over the whole sample of ~20 mm² and calculated the Mg content based on the relationship between the peak position of NBE emission and Mg content of the $Zn_{1-x}Mg_xO$ thin films [20]: $E(Zn_{1-x}Mg_xO) = E(ZnO) + 1.64*x$ (eV), where $E(ZnO)$ is the NBE emission peak of ZnO nanowires. The calculated Mg content of the ZMO nanostructures was $9.54 \pm 1.11\%$, which is close to that from XRD analysis. The blueshift of the UV emission demonstrated the band gap engineering of ZnO and further confirmed that the Mg ions had incorporated into the ZnO host lattice.

We then sought to investigate the influence of Mg doping on microscopic structures and vibrational properties for ZnMgO materials by micro-Raman spectroscopy with a fixed laser spot of about 2 μm². The RT Raman spectra of both ZMO nanostructures and ZnO nanowires are shown in Fig. 4. We can see that the Raman peak at 417 cm⁻¹ keeps unshifted in frequency that which comes from the sapphire substrate [4]. The assignments of all observed Raman lines are listed in Table 1, according to the previous Raman studies of ZnO [21–25]. It can be seen that although most of the Raman peaks from the ZMO nanostructures correspond well to those of the ZnO nanowires, the Raman spectra of ZMO nanostructures have shown their own
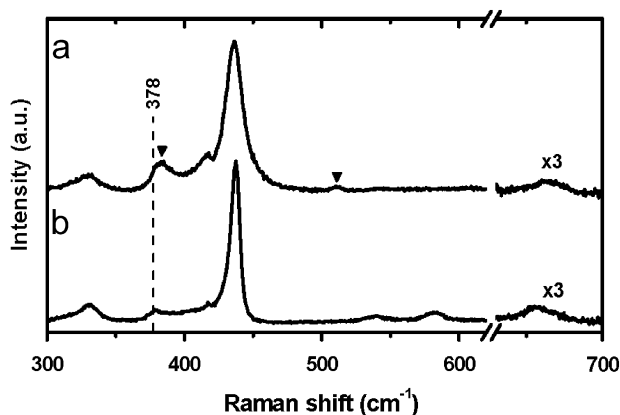
Fig. 4. The Raman spectra of ZMO nanostructures (a) and ZnO nanowires (b). Triangles denote the additional modes.

Table 1
Phonon modes frequencies in our work and tentative assignments of all the peaks

$\omega_0 (cm^{-1})$ ZMO nanostructures	$\omega_0 (cm^{-1})$ ZnO nanowires	Assingments
330	330	$E_2(high)-E_2(low)$ [24,25]
378	378	$A_1(TO)$ [35]
383	—	AM
436	438	$E_2(high)$ [23]
510	—	AM
—	540	$A_1(LO)$ [23]
—	584	$E_1(LO)$ [23]
Broad, from 640 to 680	Broad, from 640 to 680	$2[E_2(high)-E_2(low)]$ [24,25] or intrinsic host lattice defect [32]

characteristic. Firstly, it was interesting to note that $E_2(high)$ phonon lines redshifted to the lower frequency from 437.7 to 436.4 cm^{-1} and broadened (FWHM) from 8.23 to 15.3 cm^{-1} as Mg was introduced into the ZnO nanowires. Secondly, the origin of the vibration mode around 660 cm^{-1} still is controversial. Thirdly, two additional AMs around 383 and 510 cm^{-1} were detected only for ZMO nanostructures, marked as triangles in Fig. 4.

In general, as the crystal is alloying, the phonons can be confined in space, owing to the potential fluctuations of the alloy disorder, which gives rise to a relaxation of the $q = 0$ selection rule in Raman scattering [26,27]. Several groups [3,28–30] discussed the same observations in a ZnO system doped with other elements (e.g., N, Mn, Co). Therefore, the spatial phonons confinement arose from alloy potential fluctuations, as Mg^{2+} random substitution induced the microscopic structural disorder in the periodic zinc atomic sublattice and broke the translational symmetry. Chen et al. [24] and Xing et al. [25] assigned the origin of 660 cm^{-1} peak to the multiphonon processes $2[E_2(high)-E_2(low)]$ in pure ZnO nanostructures whereas Cheng et al. [31] reported this mode in ZnO:Ce nanostructures and connected it with the metastable Ce-rich solid solution

layer. In our experiments, the vibration mode around 660 cm^{-1} also is observed in ZnO nanowires; it should be an intrinsic mode of ZnO induced by Mg^{2+} substitution, which is analogous to Yang et al. [32] ascribed to intrinsic host lattice defects in Mn-doped ZnO nanostructures.

Furthermore, the AMs around 383 and 510 cm^{-1} have not been observed in the previous works for ZnMgO systems. We tentatively suggested that these two structures are likely the LVMs related to magnesium. Eq. (1) [33] gives us a rough estimate of the Mg-related LVM frequency from the effective reduced masses $\mu = (1/M + 1/m)^{-1}$ of the ZnO and LVM:

$$\frac{\omega(LVM)}{\omega(ZnO)} \approx \sqrt{\frac{\mu_{ZnO}}{\mu_{LVM}}}. \tag{1}$$

By using $\omega(ZnO–E_2(high)) = 437.7$ cm^{-1} measured from ZnO nanowires, we obtained 373 and 505 cm^{-1} for LVMs of Mg on substitutional O and Zn sites in the ZnO lattice, respectively. The calculated frequencies of LVMs for the Mg–Zn and Mg–O pairs are pretty close to the experimental values of 383 and 510 cm^{-1}. Nevertheless, the line around 510 cm^{-1} also has been observed in the Raman spectra of Fe-, Sb-, Al-, N-, and Ga + N-doped ZnO films [3,4,34]. Owing to the large differences in mass among the dopant species, this 510-cm^{-1} mode must be related to intrinsic host lattice defects rather than the above-mentioned LVM. Therefore, another possible explanation about the 510-cm^{-1} band may be attributed to the host lattice defects induced by Mg incorporation. Due to the differences in the ionic radii of Mg impurity and host ions, when Mg^{2+} ions occupy the Zn sites, some new lattice defects are introduced or intrinsic host-lattice defects become activated. As a result, some additional vibrational modes, characteristic of substitution-induced vibrations, appear in the Raman spectra that probably connect with the raised intensity of deep-level emission. The influence of atom substitution on structural disorder is being explored to investigate the reduction of grain size in ZMO nanostructures and will be addressed in future research.

4. Conclusion

In summary, the ZnMgO nanostructures with wurtzite structure were synthesized via thermal diffusion. The dependence of the lattice constant and the NBE emission at RT along with the observation of Mg-related Raman vibration on Mg incorporation confirmed Mg^{2+} substitution for Zn^{2+} lattice sites. The first-order $E_2(high)$ phonon line of ZnO:Mg nanostructures was broadened and redshifted as a result of microscopic structural disorder induced by Mg^{2+} random substitution. In addition to the host phonons of ZnO, we found two AMs at 383 and 510 cm^{-1}, which correlated with the Mg-related lattice vibrations leading to the change in ZnO host lattice.

Acknowledgments

References

[1] J.H. Lim, C.K. Kang, K.K. Kim, I.K. Park, D.K. Hwang, S.J. Park, Adv. Mater. 18 (2006) 2720.

[2] J.Y. Bae, J. Yoo, G.C. Yi, Appl. Phys. Lett. 89 (2006) 173114.

[3] A. Kaschner, U. Haboeck, M. Strassburg, G. Kaczmarczky, A. Hoffmann, C. Thomsen, A. Zeuner, H.R. Alves, D.M. Hoffmann, B.K. Meyer, Appl. Phys. Lett. 80 (2002) 1909.

[4] C. Bundesmann, N. Ashkenov, M. Schubert, D. Spemann, T. Butz, E.M. Kaidashev, M. Lorenz, M. Grundmann, Appl. Phys. Lett. 83 (2003) 1974.

[5] F.J. Manjon, B. Mari, J. Serrano, A.H. Romero, J. Appl. Phys. 97 (2005) 053516.

[6] J. Serrano, A.H. Romero, F.J. Manjon, R. Lauck, M. Cardona, A. Rubio, Phys. Rev. B 69 (2004) 094306.

[7] H.C. Hsu, Y.K. Tseng, H.M. Chang, J.H. Kuo, W.F. Hsieh, J. Crystal Growth 261 (2004) 520.

[8] H.C. Hsu, H.M. Cheng, C.Y. Wu, H.S. Huang, Y.C. Lee, W.F. Hsieh, Nanotechnology 17 (2006) 1404.

[9] B.D. Yao, Y.F. Chan, N. Wang, Appl. Phys. Lett. 81 (2002) 457.

[10] H.C. Hsu, C.Y. Wu, H.M. Cheng, W.F. Hsieh, Appl. Phys. Lett. 89 (2006) 013101.

[11] A. Ohtomo, M. Kawasaki, T. Koida, K. Masubuchi, H. Koinuma, Y. Sakurai, Y. Yoshida, T. Yasuda, Y. Segawa, Appl. Phys. Lett. 72 (1998) 2466.

[12] P. Bhattacharya, R.R. Das, R.S. Katiyar, Appl. Phys. Lett. 83 (2003) 2010.

[13] W.Q. Peng, S.C. Qu, G.W. Cong, Z.G. Wang, Appl. Phys. Lett. 88 (2006) 101902.

[14] B.P. Zhang, N.T. Binh, Y. Segawa, Y. Kashiwaba, K. Haga, Appl. Phys. Lett. 84 (2004) 586.

[15] H.C. Hsu, C.S. Cheng, C.C. Chang, S. Yang, C.S. Chang, W.F. Hsieh, Nanotechnology 16 (2005) 297.

[16] X.L. Wu, G.G. Siu, C.L. Fu, H.C. Ong, Appl. Phys. Lett. 78 (2001) 2285.

[17] B.X. Lin, Z.X. Fu, Y.B. Jia, Appl. Phys. Lett. 79 (2001) 943.

[18] K. Vanheusden, W.L. Warren, C.H. Seager, D.R. Tallant, J.A. Voigt, B.E. Gnade, J. Appl. Phys. 79 (1996) 7983.

[19] S.A. Studenikin, N. Golego, M. Cocivera, J. Appl. Phys. 84 (1998) 2287.

[20] M. Lorenz, E.M. Kaidashev, A. Rahm, Th. Nobis, J. Lenzner, G. Wagner, D. Spemann, H. Hochmuth, M. Grundmann, Appl. Phys. Lett. 86 (2005) 143113.

[21] J.F. Scott, Phys. Rev. B 2 (1970) 1209.

[22] T.C. Damen, S.P.S. Porto, B. Tell, Phys. Rev. 142 (1966) 570.

[23] R.P. Wang, G. Xu, P. Jin, Phys. Rev. B 69 (2004) 113303.

[24] S. Chen, Y. Liu, C. Shao, R. Mu, Y. Lu, J. Zhang, D. Shen, X. Fan, Adv. Mater. 17 (2005) 586.

[25] Y.J. Xing, Z.H. Xi, Z.Q. Xue, X.D. Zhang, J.H. Song, R.M. Wang, J. Xu, Y. Song, S.L. Zhang, D.P. Yu, Appl. Phys. Lett. 83 (2003) 1689.

[26] P. Parayanthal, F.H. Pollak, Phys. Rev. Lett. 52 (1984) 1822.

[27] L.Y. Lin, C.W. Chang, W.H. Chen, Y.F. Chen, S.P. Guo, M.C. Tamargo, Phys. Rev. B 69 (2004) 075204.

[28] G. Du, Y. Ma, Y. Zhang, T. Yang, Appl. Phys. Lett. 87 (2005) 213103.

[29] J.B. Wang, H.M. Zhong, Z.F. Li, W. Lu, J. Appl. Phys. 97 (2005) 086105.

[30] H.Y. Xu, Y.C. Liu, C.S. Xu, C.L. Shao, R. Mu, J. Chem. Phys. 124 (2006) 074707.

[31] B.C. Cheng, Y.H. Xiao, G.S. Wu, L.D. Zhang, Appl. Phys. Lett. 84 (2004) 416.

[32] L.W. Yang, X.L. Wu, G.S. Huang, T. Qiu, Y.M. Yang, J. Appl. Phys. 97 (2005) 014308.

[33] A. Kaschner, H. Siegle, G. Kaczmarczyk, M. Straßburg, A. Hoffmann, C. Thomsen, U. Birkle, S. Einfeldt, D. Hommel, Appl. Phys. Lett. 74 (1999) 3281.

[34] H. Harima, J. Phys.: Condens. Matter 16 (2004) S5653.

[35] B.H. Bairamov, A. Heinrich, G. Irmer, V.V. Toporov, E. Ziegler, Phys. Status Solidi B 119 (1983) 227.